# TN017: Test beam beamline resolution and systematic errors

Josh Devan & Rik Gran

July 22, 2014

**Abstract**

The low energy test beam run, performed during the Summer of 2010, required the development of a new, tertiary beamline at the Fermilab Test Beam Facility to produce, identify and momentum-analyze low energy hadrons, primarily pions and protons. This note documents the beamline hardware, reconstruction, momentum resolution and systematic errors. The systematic uncertainty on reconstructed momentum is the quadrature sum of four components: 1.0% per GeV/c for the alignment of the wire chambers, 0.5% for the alignment of the magnets, 0.5% for the longitudinal extent of the magnetic field and 0.5% for all other magnetic field errors. The errors sum to 1.0% at 500 MeV/c and 1.3% at 1 GeV/c.

## 1 Introduction

The MINER$\nu$A test beam was developed to quantify the response of single particles (primarily pions and protons) in the MINER$\nu$A detector to validate the detector simulation. The data allows for comparisons of calorimetric response, reaction cross-section, Birks' law, $\mathrm{d}E/\mathrm{d}x$ and energy scale. The test beam, in combination with external datasets, sets the systematic error on single particle response and inclusive recoil calorimetry in MINER$\nu$A analyses.

The test beam detector consists of 40 planes of $\sim$1 m$^2$ active area, identical to MINER$\nu$A planes other than dimensions and the exclusion of clear fiber cables in the readout system. The planes can be interleaved with sheets of lead and steel absorber to emulate the downstream calorimeters of the MINER$\nu$A detector.

The project required the development of a new, tertiary beamline at the Fermilab Test Beam Facility to create, identify and momentum-analyze single particles incident to the test beam detector. The beam is composed of low energy (400 MeV/c to a few GeV/c) hadrons with a small electron content. This note covers the resolution and systematic errors on the reconstructed momentum of particles in this beamline.

## 2 Physical description

The test beam beamline consists of a target and collimator and two pairs of wire chambers upstream and downstream of a pair of dipole magnets (see Figures 1 & 2). Particle momentum is reconstructed by fitting a path through the four chambers and a calculated field

Figure 1: Photograph of the test beam beamline. Secondary pions enter from the left.

map for the dipole magnets. A time-of-flight (TOF) system, consisting of an upstream scintillator paddle on the rear of the collimator and a downstream scintillator wall on the rear of wire chamber 4 (WC4), allows for particle identification. The beamline is approximately 6 m in length from upstream to downstream TOF with a 115 MeV/c transverse momentum kick delivered by the magnetic field.

The Fermilab Test Beam Facility provides a beam of secondary pions at a selected energy and intensity to impact the target. Secondary pions are created by colliding main injector protons upstream of the facility. For the Summer 2010 run, the secondary beam was tuned to 16 GeV pions at an intensity of 300 k, delivered once per minute in a 4 second window.

The four wire chambers were initially constructed for the HyperCP experiment [1]. The upstream pair are identical with an aperture of 457 mm × 254 mm and a wire pitch of 1.016 mm. The downstream pair are identical with an aperture of 559 mm × 305 mm and a wire pitch of 1.270 mm. The chambers are constructed of four wire planes, X, U, V and X'. The X and X' planes are aligned vertically with a half wire pitch offset between the two. The U and V planes are aligned at $\pm 26.6^\circ = \pm \arctan(1/2)$ from vertical. The wire pitch, measured orthogonal to the wire direction, is uniform between all planes in a chamber. The readout system for the chambers identifies only whether each wire was hit or not hit in each readout window, with no additional timing or pulse amplitude information.

Figure 2 depicts the global coordinate system. Figure 3 depicts the local coordinate system relative to a wire chamber.

## 3 Reconstruction

The beamline reconstruction begins by searching each plane of each chamber for single wire hits or two adjacent wire hits with at least 10 unhit wires to either side. Two adjacent wire hits are merged into a single virtual wire located between the two.

Local $(X, Y)$ hit positions are reconstructed by identifying wire hits in all four planes consistent with a particle crossing the chamber. The algorithm tests all combinations of wire hits, one hit for each of the four planes, for a common intersection. The intersection is marked as the hit position. The procedure is then repeated for all combinations of three

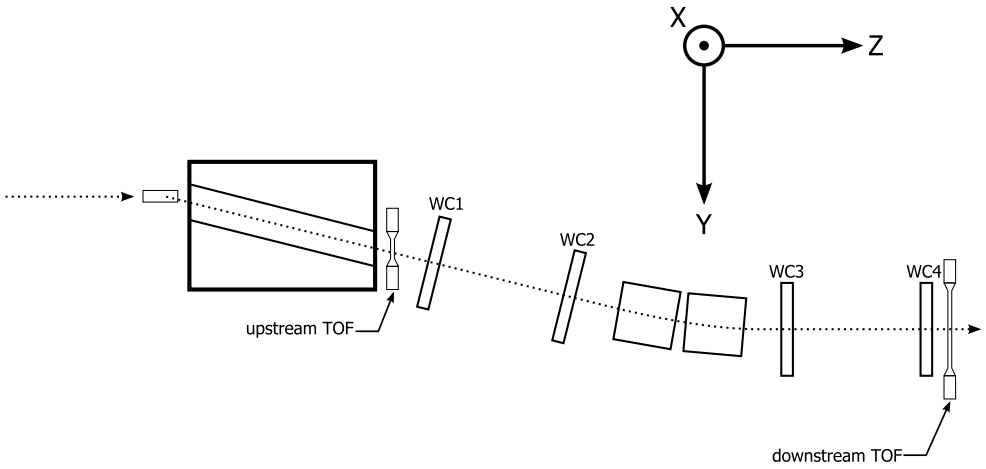


Figure 2: Top view of the test beam beamline with global coordinate system indicated. Secondary pions enter from the left.

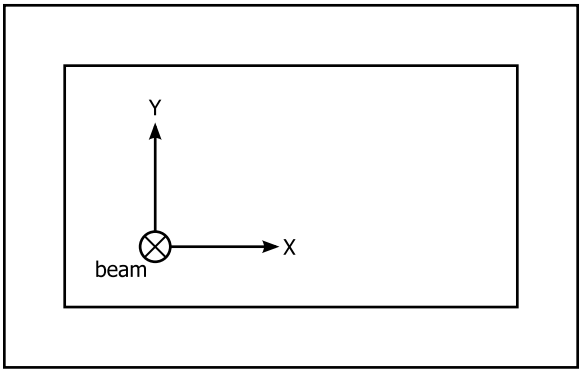


Figure 3: Local coordinate system relative to a wire chamber. Note that up is local $Y$ and global $X$; right (viewing downstream) is local $X$ and global $Y$.

planes. Multiple hits in a chamber occur often, particularly in the upstream chambers, from pile-up in the beamline. Figure 4 shows two events in the beamline; wire hits are drawn in color; reconstructed hit positions are marked with a circle.

Upstream tracks are formed from all combinations of reconstructed hit positions in the first two chambers, one hit per chamber. The tracks are projected to the collimator and magnet aperture and those falling outside are discarded. The procedure is repeated to form downstream tracks without the collimator projection.

Upstream and downstream tracks are merged by projecting to a plane in the center of the two magnets and verifying a common intersection.

Events with a single merged track are passed to the momentum fitter. The momentum fitter takes a fixed initial trajectory marked by the two upstream chambers (WC1 and WC2) and varies only the momentum as it propagates the particle through the magnetic field to minimize the residual (the distance between the point at which the fit path intersects a chamber and the observed hit position) at WC3. The propagation is performed with a Runge-Kutta stepper at 1 mm increments through a field map created by Bob Wands at Fermilab with ANSYS finite-element analysis software. The decision to fit only the residual at WC3 is explained in Section 4.

A particle mass is calculated with the fit momentum and observed time of flight from the TOF system. Offsets in the time of flight from cable length and electronic delays are calibrated per run by aligning the pion and proton mass peaks. A particle identification is performed using a combination of mass and TOF cuts to identify pions, kaons, protons, deuterons and electrons.

Events are flagged which pass a set of "loose" and "strict" quality cuts. The loose cuts require a single track passing all four chambers, a valid momentum fit (the fit converges), a maximum magnetic field error integral (the error is set non-zero in the more questionable regions of the field map) and a valid TOF reading. The strict cuts further impose a tighter magnetic field error integral, a cut on the minimum and maximum magnetic field integral and a maximum fit $\chi^2$. In the Summer 2010 run, 43% of events passed the loose quality cuts; 30% passed the strict cuts. The loose quality events are used for analyses by default, with the strict events evaluated as a systematic.

The fit momentum spectrum is plotted in Figure 5, fit momentum versus time of flight in Figure 6 and mass spectrum in Figure 7.

# 4 Momentum resolution

The momentum resolution of the beamline is limited by multiple scattering in the air and chambers and non-uniformities in the magnetic field. The deviations from the ideal path at WC4 are the quadrature sum of those at WC3 plus the multiple scattering from WC3 and the air between WC3 and WC4. For this reason, the reconstructed momentum resolution is improved by fitting only the residual at WC3. The residual at WC4 is utilized to validate the multiple scattering model and to evaluate alignment systematics (see Section 5).

The deviations from multiple scattering and field non-uniformities are modeled event by event with a Kalman filter. The Kalman filter does not model the curvature of the path through the magnetic field; it assumes a straight path with the path lengths and field integral calculated by the momentum fitter. The deviations are taken as perturbations to the ideal fit path. The straight path assumption relies on the magnetic field integral being nearly constant for the small deviations resulting from multiple scattering and field non-

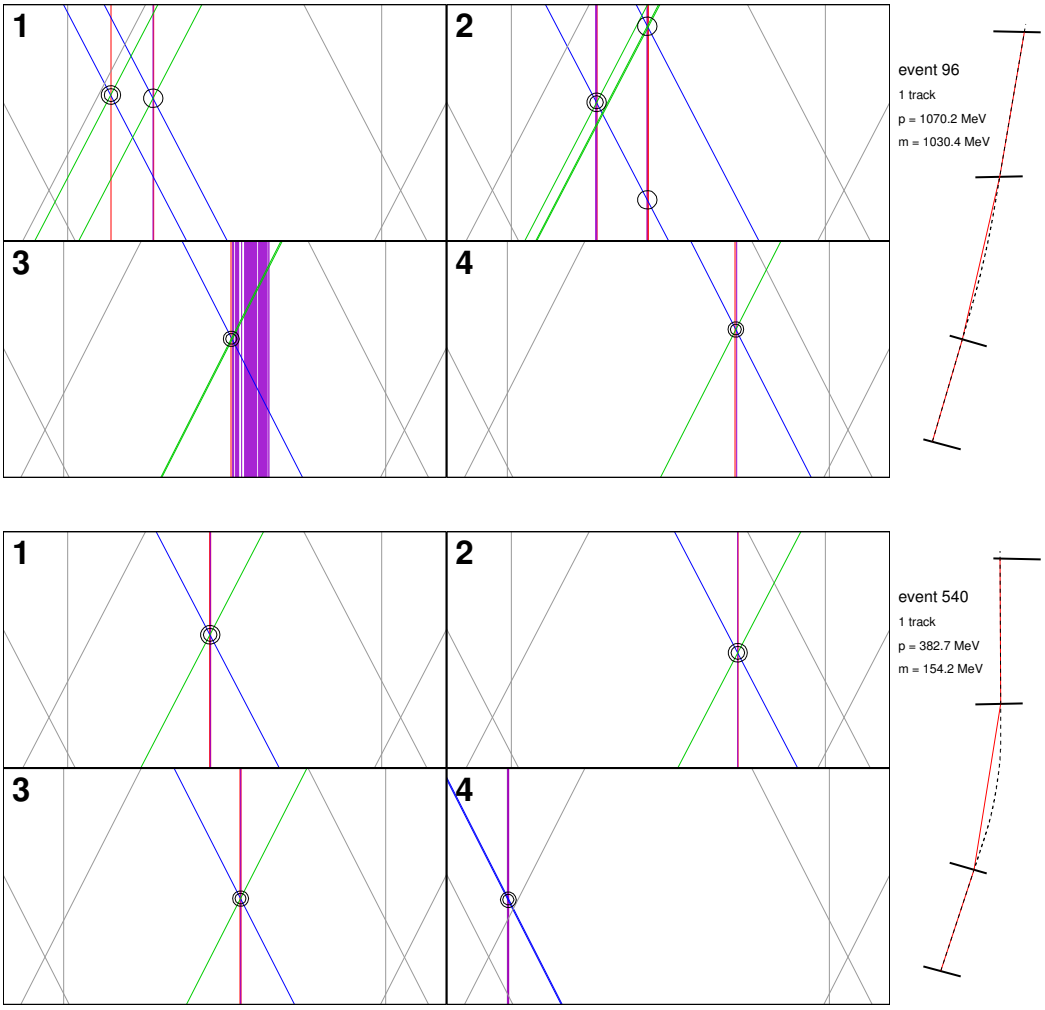


Figure 4: Beamline event displays. Wire hits are drawn in color within the four chambers; the limits of the wire planes are drawn in gray. Reconstructed hit positions are marked with a circle; the hit position incorporated in the track is marked with a double circle. On the right, a red line connects the hit position in each chamber; the fit path through the field is marked with a dashed line. In chamber 3 of the upper display, a $\delta$-ray results in a string of adjacent wire hits, which the beamline ignores and proceeds with the remaining three planes of the chamber.

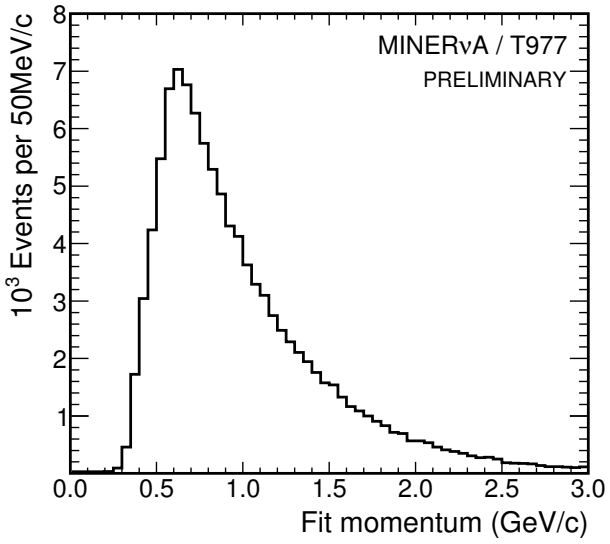


Figure 5: Fit momentum spectrum for the Summer 2010 run.

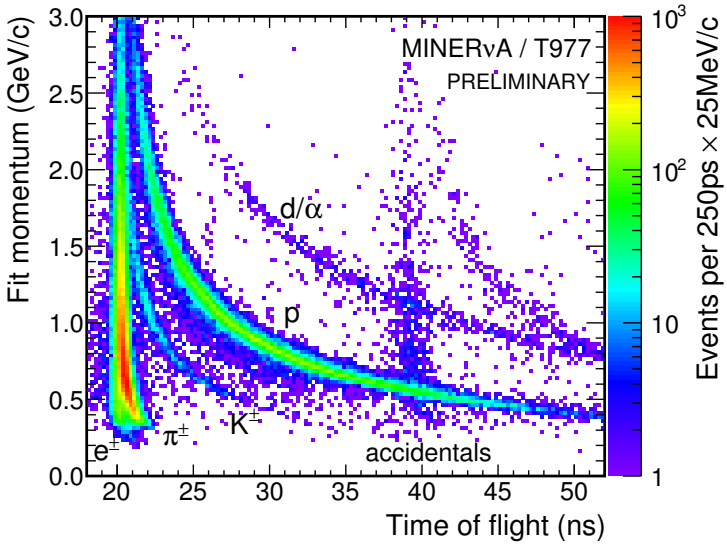


Figure 6: Fit momentum versus time of flight for the Summer 2010 run. Particle species indicated. The shadow at +19 ns is from adjacent buckets in the accelerated beam.

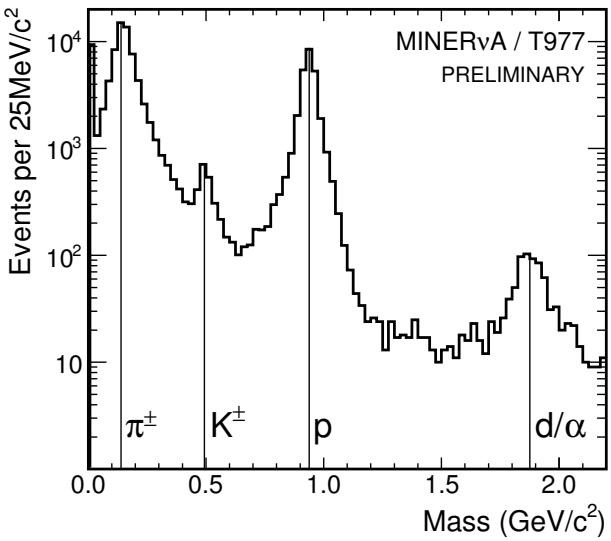


Figure 7: Mass spectrum for the Summer 2010 run. The width of the peaks is driven by the ∼250 ps resolution of the TOF system. Vertical lines are drawn at the PDG mass.

uniformities. The Kalman filter calculation is performed separately for the horizontal and vertical coordinates.

The calculation relies on a particle hypothesis and therefore must be performed after a mass is calculated. The results of the Kalman filter do not influence the momentum fit. The algorithm is run afterwards to compute the momentum resolution per event.

The Kalman filter state vector, $\mathbf{x}$, is defined as:

$$\mathbf{x} = \begin{bmatrix} x \\ \theta \end{bmatrix} \tag{1}$$

Where $x$ is the transverse position deviation from the ideal path and $\theta$ is the angle of the particle momentum vector relative to ideal. $x$ and $\theta$ are defined to be in either the horizontal or vertical plane.

The initial covariance, $\mathbf{P}_0$, is defined as:

$$\mathbf{P}_0 = \begin{bmatrix} L & 0 \\ 0 & L \end{bmatrix} \tag{2}$$

Where $L$ is a large number ($10^6$), reflecting that no information is known about the initial position or angle. The initial covariance is defined at the collimator. The Kalman filter then performs four steps to the four chambers, updating the covariance matrix with each step.

The state transition model, $\mathbf{F}$, is defined as:

$$\mathbf{F} = \begin{bmatrix} 1 & h \\ 0 & 1 \end{bmatrix} \tag{3}$$

Where $h$ is the step length from collimator to chamber or chamber to chamber as computed by the momentum fitter along the curved path. The state transition model corresponds to a simple linear projection.

The process noise covariance, $\mathbf{Q}$, is defined as:

$$\mathbf{Q} = \mathbf{Q}_1 + \mathbf{Q}_2 \tag{4}$$

$$\mathbf{Q}_1 = \begin{bmatrix} h^2\theta^2_{\text{Al}} & h\theta^2_{\text{Al}} \\ h\theta^2_{\text{Al}} & \theta^2_{\text{Al}} \end{bmatrix} \tag{5}$$

$$\mathbf{Q}_2 = \begin{bmatrix} h^2\theta^2_{\text{air}}/3 & h\theta^2_{\text{air}}/2 \\ h\theta^2_{\text{air}}/2 & \theta^2_{\text{air}} \end{bmatrix} \tag{6}$$

$\mathbf{Q}_1$ describes the multiple scattering from a chamber; $\mathbf{Q}_2$ describes the scattering from air. The chambers function as point scatterers, hence the position and angular deviation at the next chamber are absolutely correlated. For scattering in air, position and angle are only partially correlated because the scattering can occur at any point along the track. $\theta_{\text{Al}}$ and $\theta_{\text{air}}$ are the one sigma width of the angular deviation from multiple scattering by aluminum and air, respectively, given by Equation (30.15) in Section (30.3) of the PDG[2], "Multiple scattering through small angles":

$$\theta_0 = \frac{13.6\,\text{MeV}}{\beta cp} z\sqrt{x/X_0}\Big[1 + 0.038\ln\left(x/X_0\right)\Big] \tag{7}$$

Where $v = \beta c$ is the particle velocity, $p$ is the momentum, $z$ is the charge of the particle and $x/X_0$ is the thickness of the scatterer in radiation lengths. The PDG section also gives the correlations between position and angle.

The observation model, $\mathbf{H}$, is defined as:

$$\mathbf{H} = \begin{bmatrix} 1 & 0 \\ 0 & 0 \end{bmatrix} \tag{8}$$

Reflecting that only the position, not the angle, can be measured by a chamber.

The observation noise covariance, $\mathbf{R}$, is defined as:

$$\mathbf{R} = \begin{bmatrix} \text{WP}^2/N & 0 \\ 0 & 1 \end{bmatrix} \tag{9}$$

Where WP is the wire pitch scaled by a factor, $N$. For a uniform distribution of width $w$, the variance is given by $w^2/12$. For a single X plane in the chambers, we expect $N = 12$ for the uncertainty on the horizontal position (orthogonal to the wire direction). Including a single U or V plane, $N = 12/5 = 2.4$ for the vertical uncertainty (from the vertical distance between two adjacent U or V wires). The chambers, however, are constructed of multiple wire planes, so we expect better than this. In practice, $N$ dominates the expected deviations at large momentum, when multiple scattering is small, and is fit to match the data.

In the predict phase of the Kalman filter, the predicted covariance, $\mathbf{P}'$, is given by:

$$\mathbf{P}' = \mathbf{F}\mathbf{P}\mathbf{F}^{\text{T}} + \mathbf{Q} \tag{10}$$

In the update phase, the updated covariance, $\mathbf{P}$, is given by:

$$\mathbf{S} = \mathbf{H}\mathbf{P}'\mathbf{H}^{\text{T}} + \mathbf{R} \tag{11}$$

$$\mathbf{K} = \mathbf{P}'\mathbf{H}^{\text{T}}\mathbf{S}^{-1} \tag{12}$$

$$\mathbf{P} = (\mathbf{I} - \mathbf{K}\mathbf{H})\mathbf{P}' \tag{13}$$

Where $\mathbf{S}$ is the measurement covariance, $\mathbf{K}$ is the optimal Kalman gain and $\mathbf{I}$ is the identity matrix. The measurement covariance, $\mathbf{S}$, is the uncertainty between the projected and measured (fit and observed) state. $\sqrt{\mathbf{S}(0,0)}$ is the one sigma width of the residual from multiple scattering and field non-uniformities. The updated covariance, $\mathbf{P}$, is the uncertainty after including the measured hit at a chamber, but before considering scattering by that chamber.

To a good approximation, the fit momentum, $p$, is given by:

$$p = \frac{p_t}{\theta} \tag{14}$$

Where $p_t$ is the transverse momentum kick from the magnetic field, equal to the field integral times the charge of the particle and $\theta$ is the bend angle between the upstream and downstream tracks. $p_t$ is typically $\sim$115 MeV/c for unit charge particles in the beamline.

The reconstruction takes the initial particle trajectory at WC1 and WC2 as fixed and varies the momentum to minimize the residual at WC3. The fixed initial trajectory and small non-primary components (primary is global $X$) of the magnetic field force the vertical residuals at WC3 and WC4 effectively at a linear projection from upstream. By varying the momentum, the horizontal residual at WC3 will approach zero (within the limits of the momentum parameter and without negating the charge of the particle). This leaves three residuals with which to evaluate the multiple scattering and field non-uniformity model: the vertical residual at WC3 and both the horizontal and vertical residuals at WC4.

Figure 8 shows the normalized residuals (residual over one sigma uncertainty) for the three samples on the left. On the right, the one sigma width of a Gaussian fit to the residual as a function of momentum times velocity, $p \times v$, is plotted for pions (blue), protons (red) and combined (black). Multiple scattering, as calculated in Equation 7, is a function of $p \times v$, so pions and protons overlap on this plot (though protons populate the lower values as the two particles have roughly the same momentum spectrum, but the $v$ term is lower for protons). The Kalman filter prediction for the one sigma width of the residual ($\sqrt{\mathbf{S}(0,0)}$ from above) is plotted in purple.

In order to achieve agreement with the data, two parameters of the Kalman filter were tuned. The first is the scale on the wire pitch term, $N$, in Equation 9, which sets the uncertainty in the high momentum limit. For the horizontal residual, $N$ was left at the predicted value of 12. For the vertical residuals, $N$ was raised to 3, slightly better than the predicted value of 2.4. The second parameter is the inclusion of a term for the non-uniformities of the magnetic field, which is only present in the horizontal residual from the primary component of the field.

One can imagine that the calculated magnetic field map is too ideal; that the true field has non-uniformities from the composition or geometry of the steel, such as the upper or lower surface of the magnet aperture deviating from flat. These inconsistencies produce regions of high or low field. A particle traversing the field would experience more or less transverse force, causing the particle to effectively scatter. The deviations can occur anywhere along the track so we expect the correlations between position and angle to be similar to those from multiple scattering. To include field non-uniformities in the Kalman filter, the multiple scattering from air between WC2 and WC3, $\theta_{\text{air}}$ in Equation 6, was scaled for the horizontal residual. It was found that exactly doubling $\theta_{\text{air}}$ fit the residuals at WC4 observed in the beamline data.

However, when the momentum resolution implied by this was used to smear events in our data-generated MC sample, it was observed that the smearing in MC was greater than

data. The observation was made with Rik's stopping proton sample, used for the Birks' tuning analysis (see TN037, docdb:9131). The parameter was then tuned to the stopping proton sample, with the final scale factor set at 1.3. It thus under-predicts the residual at WC4.

Initially, an alternative hypothesis for the contribution of the magnetic field to the width of the residuals was proposed; that Bethe-Bloch energy loss of the particle as it traveled through air, which is not accounted for in the fit, caused the particle to be bent more or less by the field. The energy loss is a random process and thus the bend angle would be random as well. However, taking the derivative of Equation 14 with respect to $p$ indicates that the angular deviations, $\mathrm{d}\theta$, should be proportional to $1/p^2$. This relation was not observed in the data and the hypothesis was rejected.

Figure 9 shows the fit $\chi^2$, defined as the quadrature sum of the three normalized residuals. A fit to the data finds the number of degrees of freedom to be nearly 3, as expected from the sum of three Gaussians of unity width.

An uncertainty on the fit momentum is calculated for each event by taking the derivative of Equation 14 with respect to $\theta$:

$$\mathrm{d}p = -\frac{p_t}{\theta^2}\mathrm{d}\theta = -\frac{p^2}{p_t}\mathrm{d}\theta \tag{15}$$

$p_t$ is computed by the field integral from the momentum fitter. $\mathrm{d}\theta$ is taken to be the one sigma width of the horizontal residual at WC3 ($\sqrt{\mathbf{S}(0,0)}$) divided by half the path length from WC2 to WC3. If you imagine the downstream track rotating as a result of the uncertainty at WC3, this places the pivot point at roughly the center of the two magnets. The half path length assumption was confirmed with a sample in which the hit position at WC3 was explicitly shifted in the reconstruction by the uncertainty and a new momentum was fit. Figure 10 shows the absolute (left) and fractional (right) momentum uncertainty as a function of momentum. Multiple scattering and field non-uniformities limit the momentum resolution to a few percent, but contribute no systematic bias.

# 5 Alignment systematic error

The analysis of the alignment of the wire chambers in the tertiary beamline is a twofold problem. The first is the internal alignment; the relative positions of the four planes within a chamber and the position of those planes within the frame of the chamber. The second is the external alignment; the positions of the chambers within the hall, in particular, relative to the detector.

The relative alignment of the four planes within a chamber can be validated for the horizontal axis (the more important axis in calculating particle momentum) by comparing the local $X$ coordinate computed only from the X plane, the X' plane or a combination of the U and V planes. The difference in local $X$ for each combination of planes versus the particle's angle of incidence is plotted in Figure 11. This plot contains an angle of incidence correction which accounts for the planes of the wire chamber being separated in $Z$, along the particle's trajectory. The angle of incidence correction corrects to $X$ at the center of the chamber, between the U and V planes (the planes are stacked X, U, V, X'). The deviations plane to plane are $\sim$0.2 mm at worst.

The positions of the wire chambers within the hall were surveyed at three points on the frame of the chamber. One method of evaluating the uncertainty on momentum arising from alignment is to shift the chambers in the reconstruction and observe the change

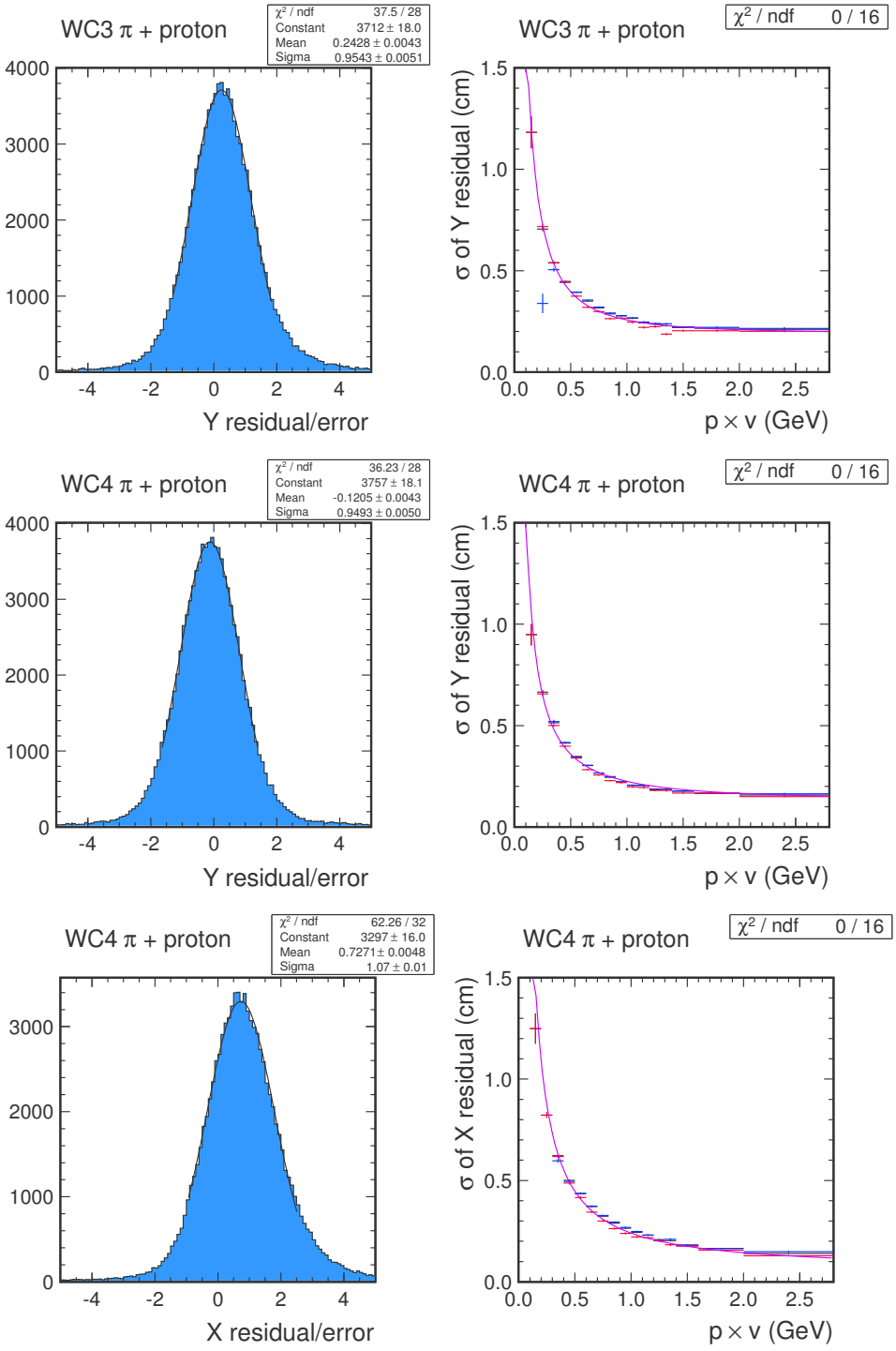


Figure 8: WC3 and WC4 residuals ($X$ is horizontal, $Y$ is vertical). Left: Normalized residual with a Gaussian fit. Right: One sigma width of a Gaussian fit to the residual as a function of $p \times v$ for pions (blue), protons (red) and combined (black) with the Kalman filter prediction in purple.

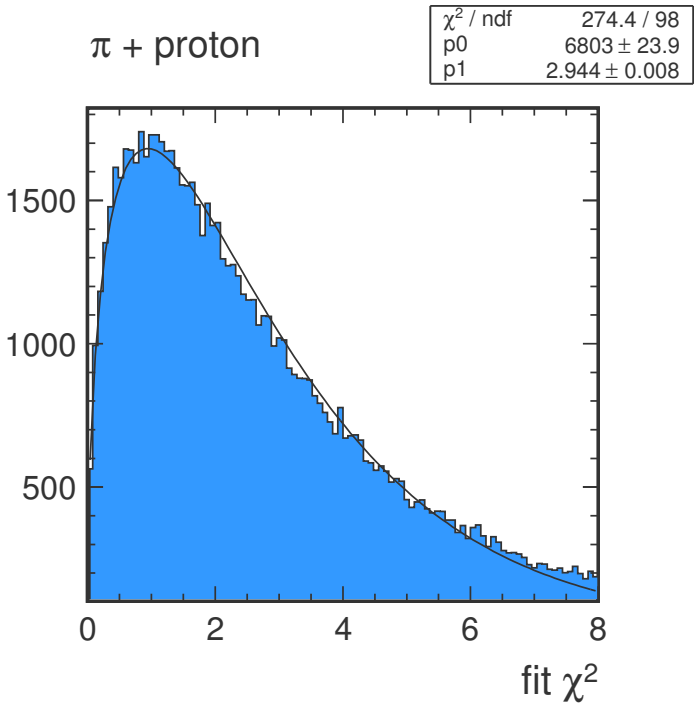


Figure 9: Fit $\chi^2$, defined as the quadrature sum of the normalized residuals at WC3 (vertical) and WC4 (horizontal and vertical). The data is fit to a $\chi^2$ distribution; p0 is a scale, p1 is the number of degrees of freedom, which is ∼3 as expected.

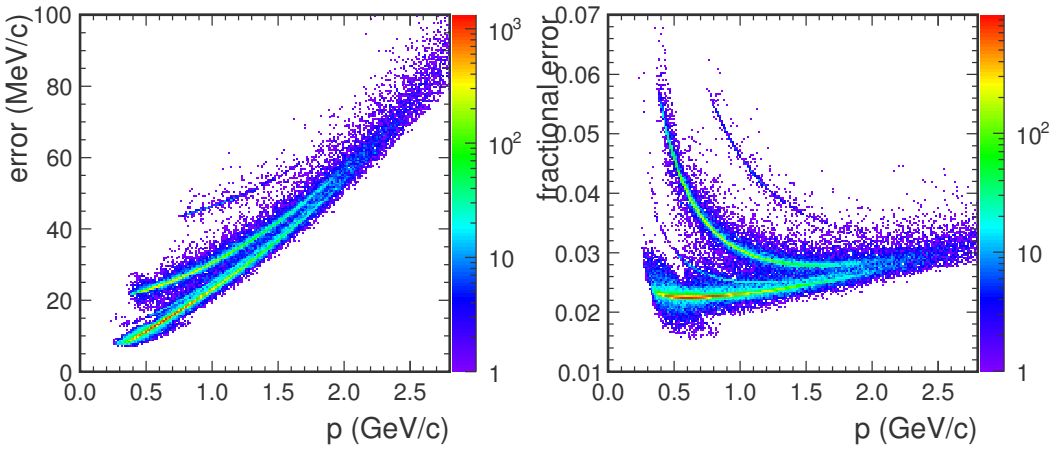


Figure 10: Absolute (left) and fractional (right) error on the reconstructed momentum from multiple scattering and magnetic field non-uniformities. The bands correspond to particle species, with the lowest error on pions, then kaons, protons and deuterons.

in reconstructed momentum. The strongest effect is observed by shifting WC2 by 1 mm, resulting in a momentum-dependent uncertainty of 2.1% per GeV/c.

The uncertainty can be further constrained by making use of three data samples:

1. **Magnet off, beam muons** – With the beam dump in place, the detector is sprayed with muons resulting from pion decays in the secondary beam. This sample was primarily used in the energy scale calibration of the detector, but we also triggered events in the beamline. The muons travel along the global $Z$ axis, intersecting chambers 2, 3, and 4. Figure 12 plots the residual observed at WC2 from the projection of WC3 and WC4. The statistics are very low in this sample.
2. **Magnet off, tertiary beam particles** – We recorded a small set of tertiary beam particles with the magnets disabled. These emerge from the collimator and pass through chambers 1, 2 and 3. Figure 13 shows the residual observed at WC3 from the projection of WC1 and WC2.
3. **Magnet on, tertiary beam particles** – This sample is, obviously, the highest statistics, but is complicated by the curvature of the particle trajectory through the magnetic field. Figure 14 plots the residual observed at WC4, defined as the intersection of the path from the momentum fitter minus the observed hit.

We cannot determine a unique set of alignment corrections from this data. A shift of any one chamber is degenerate with shifting the other three in the opposite direction. Translations and rotations of the entire beamline will not affect the observed residuals or calculated momentum. Vertical translations have a negligible affect on momentum, so we restrict ourselves to horizontal alignment. The chambers were surveyed at three points on the frame, separated by $\sim$0.5 m, so we can take uncertainties on the angles of the chamber as negligible.

To align the beamline, we restrict ourselves to only shifting two chambers. A third could be effectively shifted by fixing the position of the fourth and rotating the entire beamline, which has no affect on momentum. In practice, it is chosen to align the two upstream chambers so that the projections of tracks onto the detector, set by the two downstream chambers, is not affected. The projected tracks have previously been aligned by observing the trajectories of particles in the detector relative to the projection from the beamline.

The final alignment correction of WC2 is set by the beam muon data, 1.3 mm along the local $X$ axis. The position of WC1 was then shifted to align the tertiary beam data, both magnet on and off. The final alignment correction of WC1 is identical to WC2, 1.3 mm. This might allude to the relative alignment of the planes within the chamber frame; the two upstream chambers are identical, but different than the two identical downstream chambers.

The change in reconstructed momentum after performing the alignment is momentum-dependent, 1% per GeV/c, which is taken as the systematic uncertainty.

The final uncertainty of the beamline alignment is the position of the dipole magnets relative to the chambers. This was evaluated by shifting the magnets 5 mm along the beam axis resulting in a momentum shift of 0.5%, taken as the uncertainty.

# 6 Magnetic field systematic error

The magnetic field map used to reconstruct the data is based on a finite-element calculation done by Bob Wands using the specs for our two magnets. The calculation is further

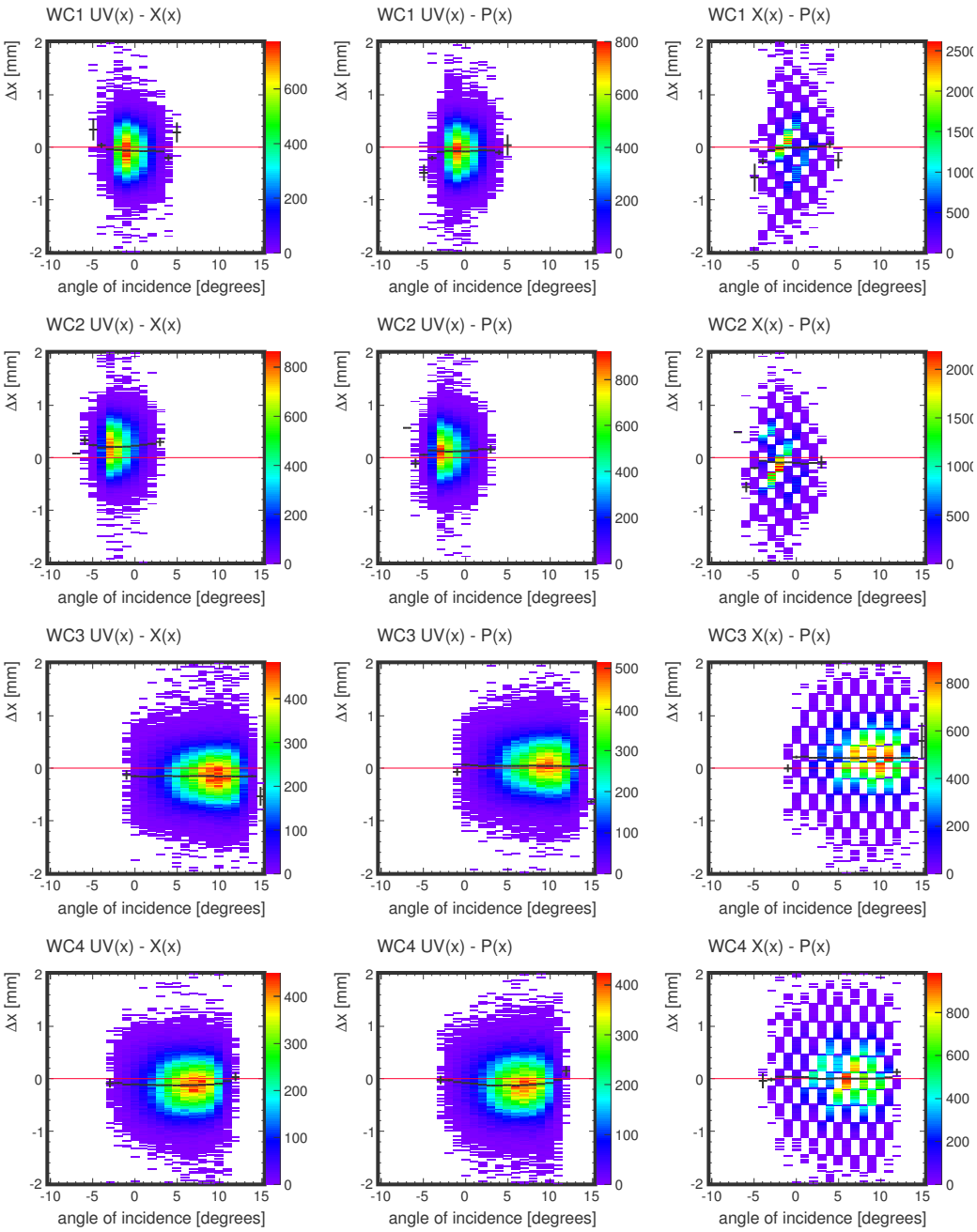


Figure 11: Relative alignment of the four planes within the four wire chambers, plotted as the difference in local $X$ (horizontal) calculated from the X plane, U & V planes and X' plane (labeled "P" in the titles) versus angle of incidence after the angle of incidence correction. The profile of the distribution is shown in black. The checkered pattern on the right occurs because the difference in X and X' is limited to discrete multiples of the wire pitch, but is shifted and smeared by the angle of incidence, binned on the horizontal axis of the plot.

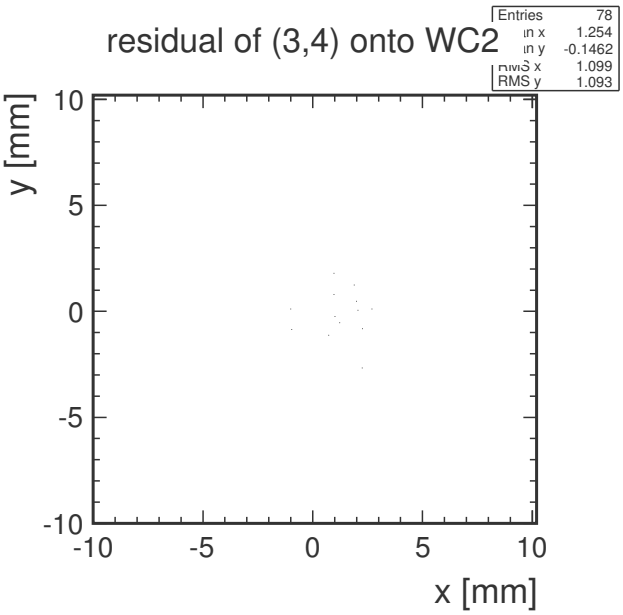


Figure 12: WC2 residual for beam muon, magnet off data. The vector from WC3 and WC4 is projected onto WC2 and the difference to the observed hit plotted. (Please pardon the 1 pixel histogram markers).

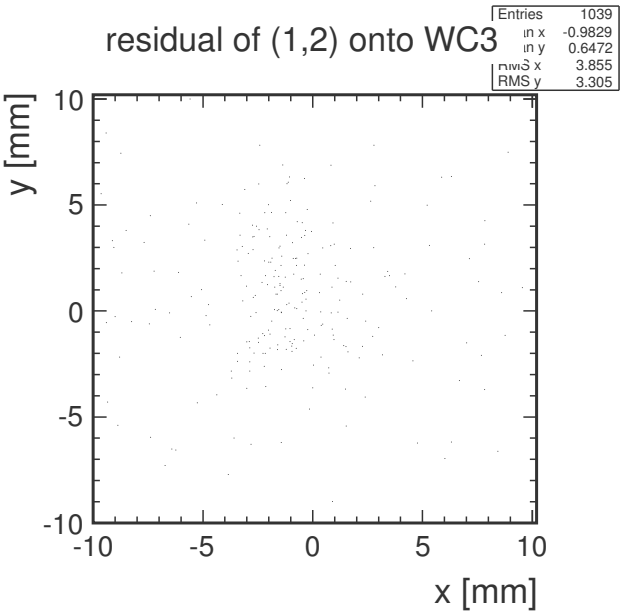


Figure 13: WC3 residual for tertiary beam, magnet off data. The vector from WC1 and WC2 is projected onto WC3 and the difference to the observed hit plotted. (Please pardon the 1 pixel histogram markers).

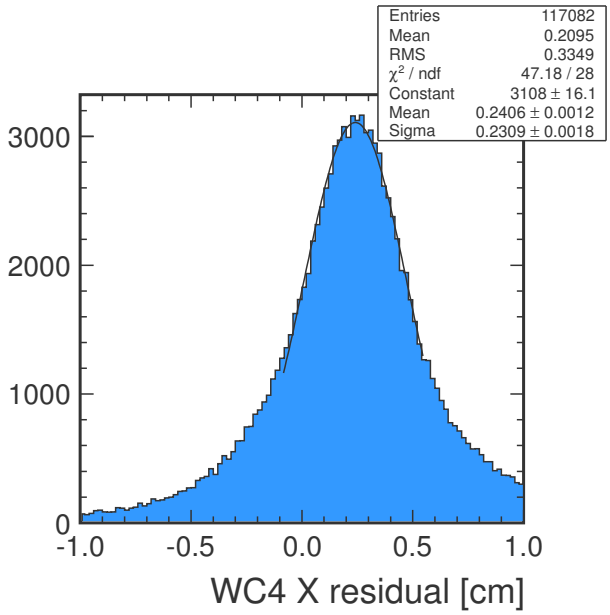


Figure 14: WC4 horizontal residual for tertiary beam, magnet on data. The residual is the intersection from the momentum fit minus the observed hit.

constrained and systematic uncertainties are evaluated using constraints from a field mapping campaign. This document presents a high level summary of the field map and its uncertainties.

More details of the evolution and analysis of this topic can be found in in several documents. The most complete is docdb:8067 there is a summary of an earlier roll-up of systematic uncertainties. The description of the field map in that document is accurate and contains more detail than what we summarize here, the description of alignment uncertainties is superceded by material elsewhere in this document. There are references to earlier notes that describe progress toward these final results.

The main effect on the reconstructed momentum is the field integral from the field map. There are two rules of thumb:

**left hand thumb** the field map (or field scale) with a larger field integral produces a larger estimate of the momentum.
**right hand thumb** all paths through the magnet give approximately the same field integral, even if they pass through regions of the field that are wildly different than another path.
**right hand rule** don't forget the right hand rule, or you will mistakenly expect to see protons in the negative focused beam. (Testbeam inside joke.)

Figure 15 illustrates the field integral of the first two pions that pass the cuts from the 20ECAL20HCAL Pi+ run. They take two very different paths through the magnetic field, but the field integral between the two is within 0.3%. The blue path, with what I call the "devil's horns" is typical for a particle that took a path that was vertically quite distant from the center; this one was about 6 cm away by the time it got to WC3. These are places

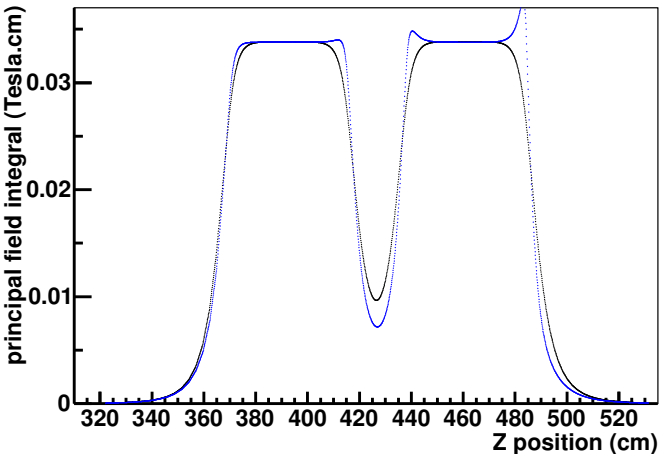


Figure 15: (In color) A demonstration of paths through the magnets for the first two pions in run 209_0001. The blue one ( the one with the devil horns on the downstream magnet is event event 209/1/6 momentum 683.4 reco mass 103.8 209/1/1 momentum 585.1 MeV/c reco mass 143.8) took a rising path through the magnets while the black one (209/1/1 momentum 585.1 MeV/c reco mass 143.8) took a relatively level path through the middle. Despite the obviously different field experienced along the path, the field integral is the same within 0.3% for the two paths.

in the region where the field changes dramatically, producing spikes in the field that are tens of percent different.

The similarity of the field integral for most events, and the systematic differences among them are shown in the contour plot Fig. 16. Typical paths are peaked around 38.3 Tesla cm. The contour scale in this figure is adjusted to better show the peak at the expense of illustrating the tails; variations of 4% cover 90% of the distribution, and our loose cuts accept events within 10% of the central field integral.

The previous figures and rules of thumb are adequate to understand how systematic uncertainties in the field contribute to systematic uncertainties in the momentum assigned to each particle and to the sample as a whole.

From the field map itself, the two most clear systematics are the absolute magnitude of the field and the longitude dimension of the magnets, both of which are constrained using data from our mapping campaign.

The entire calculated field map is scaled down by a factor of 0.9942 to bring it in line with the measured field map in the center of the magnets, and then scaled up again by a factor of 1.003 to account for operating the beam at a higher current than was used for the mapping. The calibration of the Hall probe and the stability of the magnet current means these adjustments are accurate to 0.2%.

Importantly, this calibration removes a whole class of uncertainties from the problem, compared to using just the ab initio calculation. Almost all systematics produce a change in the field at the center of the magnet and changes in the shape of the field away from the center that produce higher or lower field integrals. Because of the mapper constraint,

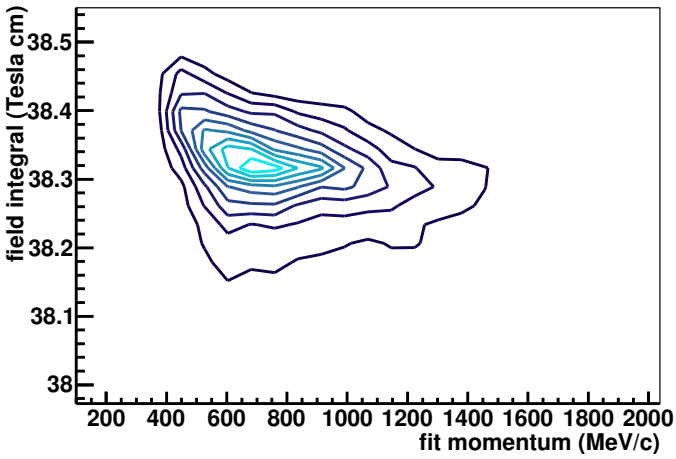


Figure 16: (In color) A demonstration of how the field integral and path through the magnet depends slightly on the momentum of the particle being reconstructed. The lowest momentum particles experience the most significant bend and have slightly longer paths through the magnets. The contour scale is adjusted to show the peak.

only changes in the shape that also produce changes in the field integral that affect the momentum reconstruction.

After this, the least constrained aspect of the magnetic field is the longitude extent of the magnet. The profile of downstream magnet from data (black) and from the calculated field (blue) is shown in Fig. 6. There is a discrepancy that shows up most clearly at the falling edge, around 0.3 meters from center, and corresponds to 2.6 mm of additional width, with the calculated field being slightly longer than the measured field. When this is combined with the reduction in uncertainty from scaling the central field, the resulting shape means the calculated field gives 0.5% additional field integral, and therefore reports a momentum that could be too high.

Because the field mapping was done with pegboard and without precision alignment, this 2.6 mm discrepancy is consistent with the tolerances of the mapping procedure. We don't take a correction for this discrepancy with a smaller error, but rather we use this 0.5% as the total systematic due to this effect. For the analysis of test beam data, this precision is already good; if more precision were needed, we would undertake an additional mapping campaign to reduce this uncertainty.

There are a wide variety of other systematic uncertainties that were studied and are reported in docdb:8067. When combined, they yield another 0.5% systematic uncertainty, which we take in quadrature to the longitude effect above.

- narrow the magnet 5mm vertically 0.3%
- narrow the magnet width 5mm horizontally 0.06% at high momentum.
- shift magnets closer in Z by 5mm = 0.17%
- effect of map granularity mean 0.01% rms 0.15%, but use the finer grained map.

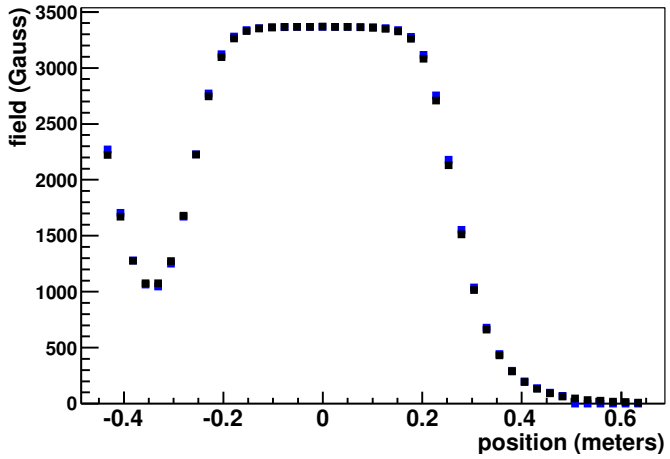


Figure 17: (In color) A demonstration of possible discrepancies in the longitude dimension of the magnet. This is from the 1H zip of the downstream magnet. Its hard to see, but at the right and left downgoing edges of the magnet, the blue (Wands' field) is higher than the black (data) by a few tens of Gauss, corresponding to between 2 and 3 mm of additional width in the blue field.

- different BH curve = 0.3%
- non-principle components = 0.1%
- field cutoff chosen and checked to be negligible.
- use simple superposition instead of a two-magnet calculation 0.5%
  sanity check, not an uncertainty

# 7 Systematic error summary

The systematic errors on reconstructed momentum are summarized in Table 1.

| | |
|---|---|
| wire chamber alignment | 1.0% per GeV/c |
| magnet alignment | 0.5% |
| magnetic field longitudinal extent | 0.5% |
| other magnetic field errors | 0.5% |
| quadrature sum | 1.0% at 500 MeV/c, 1.3% at 1 GeV/c |

Table 1: Summary of systematic errors on reconstructed momentum.

# References

[1] R.A. Burnstein, et al., NIM A 541 (2005) 516.

[2] J. Beringer, et al. (Particle Data Group), Phys. Rev. D 86 (2012) 010001.